Rare Metal Materials and Engineering
Volume 50, Issue 12, December 2021
Available online at www.rmme.ac.cn

Science Press

Cite this article as: Xu Yang, Ke Liming, Mao Yuqing, et al. Effect of Rotational Speed on Intermetallic Compounds and Low Melting Point Eutectic of Al/Mg Friction Stir Welded Joints[J]. Rare Metal Materials and Engineering, 2021, 50(12): 4209-4217.

ARTICLE

Effect of Rotational Speed on Intermetallic Compounds and Low Melting Point Eutectic of Al/Mg Friction Stir Welded Joints

Xu Yang[1], Ke Liming[1,2], Mao Yuqing[2], Chen Yi[2]

[1] State Key Laboratory of Solidification Processing, Northwestern Polytechnical University, Xi'an 710072, China; [2] National Defense Key Discipline Laboratory of Light Alloy Processing Science and Technology, Nanchang Hangkong University, Nanchang 330063, China

Abstract: The effects of rotational speed on the intermetallic compounds and low melting point eutectic of Al/Mg friction stir welded joints were investigated. The interfacial microstructures of both Al and Mg sides were characterized by electron backscatter diffraction. The results show that when the low rotational speed of 375 r/min is used, the eutectic layer ($Mg+Al_{12}Mg_{17}$), with an average thickness of 38.83 μm, appears at the upper of the Mg side interface. A continuous columnar Al_3Mg_2 layer with a thickness of 12.3 μm, perpendicular to the boundary between the Al_3Mg_2 layer and eutectic layer, is also found at the upper of the Mg side interface. At the middle and bottom of the Mg side interface, there are merely Al_3Mg_2 layer and $Al_{12}Mg_{17}$ layer, the thickness of which decreases sequentially from the upper to the bottom along the thickness direction. In addition, the Al_3Mg_2 layer with high kernel average misorientation at the Al and Mg side interface provides a path for the diffusion of Al and Mg atoms. When the high rotational speed of 600 r/min is used, the eutectic layer composed of Mg solid solution and $Al_{12}Mg_{17}$ phase is distributed across the Mg side interface along the thickness direction, and the thickness of the eutectic layer increases significantly compared with that at the low rotational speed of 375 r/min. The average thickness of the Al_3Mg_2 layer and eutectic layer on the upper of the Mg side interface is 32.89 and 68.92 μm, respectively. Finally, the strain rate caused by rotational speed plays an important role in the growth of intermetallic compounds.

Key words: intermetallic compounds; low melting point eutectic; Al/Mg joints; friction stir weld; rotational speed

The hybrid structure of aluminum (Al) and magnesium (Mg) alloys has attracted much attention due to their lightweight and green recycling[1,2]. Realizing the reliable joining between Al alloy and Mg alloy has become a hot spot at present. However, conventional fusion weld will cause pores, hot cracks, and massive brittle intermetallic compounds (IMCs) because of the high heat input[3]. Friction stir welding (FSW), proposed by The Welding Institute (TWI) in 1991, is reconsidered as a solid-state joining method with low heat input[4]. To date, dissimilar FSW of Al alloy to Mg alloy has been investigated extensively[5-9]. Nevertheless, during the Al/Mg FSW process, a large amount of materials are mixed and sheared, which promotes the diffusion between the Al and Mg atoms[10]. Therefore, some intermetallic compounds (IMCs), such as Al_3Mg_2 and $Al_{12}Mg_{17}$, are inevitably formed in the Al/Mg joints. These IMCs are fragile and brittle and detrimental to the mechanical properties of the joint[11].

Azizieh et al[12] reported that Al/Mg joints with 3 mm in thickness during the FSW are easily exposed to the peak temperature of 400~500 °C. According to the Al-Mg binary phase diagram, the two kinds of eutectic temperatures are 437 and 450 °C, which are easily reached during the FSW. For example, Sato et al[13] welded a 6 mm thick plate of 1050 Al and AZ31 Mg and found that the stir zone contains massive eutectic microstructure of $Mg+Al_{12}Mg_{17}$. Mclean et al[14] conducted the dissimilar FSW for a 12 mm thick plate of AZ31B Mg and 5083 Al. At the interface of this dissimilar joint, there is a divorced lamellar eutectic consisting of Mg and $Al_{12}Mg_{17}$. For other dissimilar metals, for instance, Al/Cu, it is also reported that the eutectic reaction occurs due to high

Received date: December 21, 2020
Foundation item: National Natural Science Foundation of China (51874179, 52005240)
Corresponding author: Ke Liming, Ph. D., Professor, National Defense Key Discipline Laboratory of Light Alloy Processing Science and Technology, Nanchang Hangkong University, Nanchang 330063, P. R. China, E-mail: liming_ke@126.com

welding temperature[15]. The presence of low melting eutectics can cause the liquation crack, which is harmful to obtain a complete dissimilar joint[16]. But these literatures focus on the effect of the IMCs on the dissimilar Al/Mg joints and ignore the role of the low melting point eutectics.

Generally, for thick plate FSW, excessive frictional heat will be generated dued to a large contact area between the shoulder and the base material. Thick plate Al/Mg FSW is prone to produce low melting eutectic and brittle IMCs. Yu[17] and Kwon et al[8] reported that the rotational speed has an important influence on the heat generation and weld formation. Therefore, in this study, Al and Mg plates with 20 mm in thickness were used as base material (BM) to investigate the evolution of IMCs and low melting point eutectic under low rotational speed and high rotational speed.

1 Experiment

In the present work, 5A06 Al and AZ31B Mg plates (150 mm×60 mm×20 mm) were joined by FSW. The nominal chemical compositions of 5A06 Al and AZ31B Mg are listed in Table 1. A grooved shoulder with a diameter of 40 mm was used, and the root diameter, tip diameter and length of the thread pin were 14, 6 and 19.5 mm, respectively. The Al plate and Mg plate were placed on advancing side (AS) and retreating side (RS), respectively. To control the content of Al and Mg, an inclined butt joint was employed, and the faying surface was parallel to the outer edge of the pin (Fig.1a). The outer edge of the pin was offset by 0.5 mm from the Mg side (Fig. 1a). The thermal cycle during the FSW process was obtained by thermocouple, as shown in Fig. 1b. Due to the characteristic of heat conduction of thick plate FSW, the welding speed in this experiment was fixed at a low value of 23.5 mm/min. The low and high rotational speeds were set as 375 and 600 r/min, respectively.

The morphology and chemical composition of Al/Mg interface were analyzed by scanning electron microscopy (SEM) equipped with energy dispersive spectroscopy (EDS). Electron backscatter diffraction (EBSD) was performed to characterize the interfacial microstructure across the cross-section of the Al/Mg joint. EBSD samples were prepared using an argon ion cross-section polisher, and Channel 5 software was used for data processing.

2 Results

2.1 Thermal cycle

Fig. 2 shows thermal cycle curves of the Al side and Mg side interface at low and high rotational speeds. As previously mentioned in Fig.1b, the thermocouples were placed near the interface and marked from P1 to P6. As can be seen from Fig.2a, the peak temperatures of the upper, middle and bottom of the Al side interface are 441.9, 442.5 and 445.7 °C, respectively. The maximum temperature difference between the upper and the bottom is only 3.8 °C. On the Mg side interface, the peak temperatures of the middle and bottom are also relatively close, and the difference is only 3.2 °C. As the rotational speed increases to 600 r/min, the peak temperatures of the upper, middle and bottom of the Al side interface also increase to 459.2, 460.0 and 460.3 °C, respectively. Moreover, the peak temperature of the Mg side interface also increases with increasing the rotational speed. The peak temperature of the middle of Mg side interface reaches to 461.3 °C, as shown in Fig. 2b. It can be known from the Al-Mg binary phase diagram that the eutectic reaction will occur when the temperature exceeds 437 and 450 °C[18].

Fig.2c shows the effect of the rotational speed on the peak temperature and residence time. Here merely P2 position is used as the object of detailed description. It can be seen that when the rotational speed increases from 375 r/min to 600 r/min at the same position, the peak temperature increases from 449.8 °C to 461.3 °C, and the high temperature residence time also increases from 29 s to 47 s. Generally, the process parameters such as rotational speed and welding speed are coupled to influence the heat generation. For Al/Mg dissimilar FSW, the heat generation is significantly important to weld formation, since it is not only related to the formation of IMCs, such as Al_3Mg_2 and $Al_{12}Mg_{17}$, but also affects the formation of low melting eutectics[13,19].

An interesting phenomenon is that the peak temperatures of the AS (Al side) and the RS (Mg side) are very close, and the maximum difference is only 5.2 °C, which is inconsistent with the thin plate Al/Mg FSW joints at the same material position[20-22]. Two possible reasons are responsible for this difference. On the one hand, thick plate FSW with a lower welding speed has sufficient time to bring more high-temperature Al metal from the AS to the RS, which accumulates on the RS, as can be seen in Fig.3. On the other hand, heat conductivity of 5A06 Al is much larger than that of AZ31B Mg, and more friction heat generated by stir action is dissipated by the nearby metal of Al side instead of the Mg side.

2.2 Macrostructure

Fig. 3 presents the top-surface and cross-section morphologies of the Al/Mg joints at 375 and 600 r/min. A defect-free and smooth-surface joint is formed at 375 r/min, as can be seen from Fig. 3. In addition, the cross-sectional morphology at 375 r/min shows that there are several obvious interfaces, marked as yellow dashed line and red dashed line. From the weld nugget zone (WNZ), dark and light grey phases are distributed in the WNZ, which indicate the enough mixing of Al and Mg. The zone between the WNZ and the Mg side

Table 1 Nominal chemical compositions of AZ31B Mg and 5A06 Al plates (wt%)

Plate	Al	Zn	Mn	Si	Cu	Fe	Ni	Mg
AZ31B Mg	2.5~3.5	0.6~1.4	0.2~1	≤0.1	≤0.05	≤0.005	≤0.005	Bal.
5A06 Al	Bal.	≤0.2	0.5~0.8	0.4	0.1	≤0.4	0.1	5.8~6.8

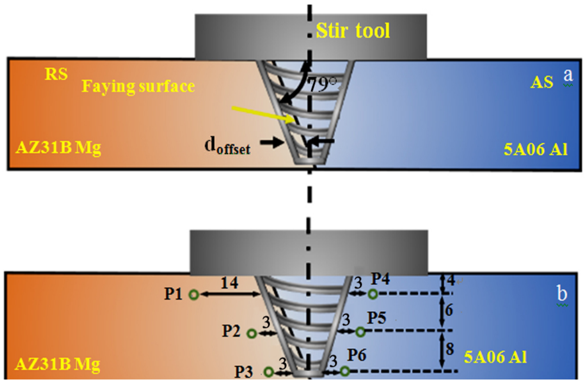

Fig.1 Schematic diagrams of Al/Mg FSW: (a) pin offset and (b) temperature measurement

interface is deformed Al zone, which migrates from the AS to the RS under the action of the pin. However, the joint at 600 r/min fractures along the Mg side interface. Compared with the joint at 375 r/min, the size of the WNZ is larger and the mixing of Al and Mg is also more enough because of the higher rotational speed. The microstructures at 375 and 600 r/min will be discussed in detail in Section 2.3.

2.3 Microstructure evolution

2.3.1 Low rotational speed

Fig.4 shows the microstructures of as-received 5A06-H112 Al alloy and AZ31B-O Mg alloy. The grains of the 5A06-H112 are in the shape of elongated ellipses, and small plate shaped $FeMnAl_6$ precipitates that are scattered throughout the microstructure are observed[23]. The microstructure of the AZ31B-O Mg alloy reveals mainly equiaxed grains.

Fig.5 shows the SEM images of the Al side interface along the thickness direction at 375 r/min. As can be seen in Fig.5a, the thermo-mechanically affected zone (TMAZ) at the upper of the Al side interface consists of coarse and deformed Al grains. According to the quantitative results of EDS in Table 2, the possible bulk Al_3Mg_2 phases and broken Al particles appear at the upper of the WNZ. It is noticed that the middle and bottom of the WNZ near the Al side interface present both Al grains instead of coarse Al_3Mg_2 phase. The size of Al grain at the bottom of the WNZ is smaller than at the middle of the WNZ, as shown in Fig.5b and 5c.

Fig. 6 presents the EBSD phase distribution maps and the kernel average misorientation (KAM) maps along the thickness direction. The phases marked as red and yellow are Al and Al_3Mg_2, respectively. The EBSD phase maps in Fig.6a also confirm the existence of the bulk Al_3Mg_2 phase with the diameter exceeding 68.45 μm. However, the fine Al_3Mg_2 phases appear at the middle of the WNZ instead of the Al side interface, as shown by the white dotted circle in Fig.6b. Fig.6c shows that the Al_3Mg_2 phase does not exist at the bottom of the Al side interface and the WNZ.

Compared with the lath-shaped grains of the as-received 5A06 Al (Fig.4a), the grain of the middle of the WNZ near the Al side presents a significantly refined and equiaxed shape. As shown in Fig. 6a~6c, high angle grain boundaries (HAGBs) having a misorientation beyond 15° are displayed as blue lines and low angle grain boundaries (LAGBs) having a misorientation between 2° and 15° are displayed as black lines. It can be noted that majority of the grain boundaries in the WNZ near the Al side are surrounded by HAGBs, as shown in Fig.7a and 7b. In as-received 5A06 Al, the LAGBs of 2°~15° occupy 78.3%, and the HAGBs beyond 15°account for 21.7%[23]. The HAGBs in the WNZ increase significantly, indicating that most of the original LAGBs in the BM are transferred into the HAGBs during the FSW due to the continuous dynamic recrystallization (CDRX)[24].

In addition, the middle of the TMAZ on the Al side shows partially elongated large grains, while the bottom consists of fine equiaxed grains, as shown in Fig.6b and 6c. It can be seen from Fig. 7c and 7d that the fraction of the HAGBs in the bottom of the TMAZ also increases to 57% and 42%, respectively, but it is much smaller than that of the WNZ. The vibration of the HAGBs and grain size in the TMAZ indicates that partial dynamic recrystallization and dynamic recovery occur in the TMAZ due to high temperature and deformation[25,26].

The KAM map depicts the density of dislocation, in which high KAM value indicates more local misorientation[27]. As shown in Fig.6d, an average KAM value of 0.6074 is obtained at the Al_3Mg_2 phase, indicating that the Al_3Mg_2 layer has higher strain than the surrounding Al grains. The high strain of

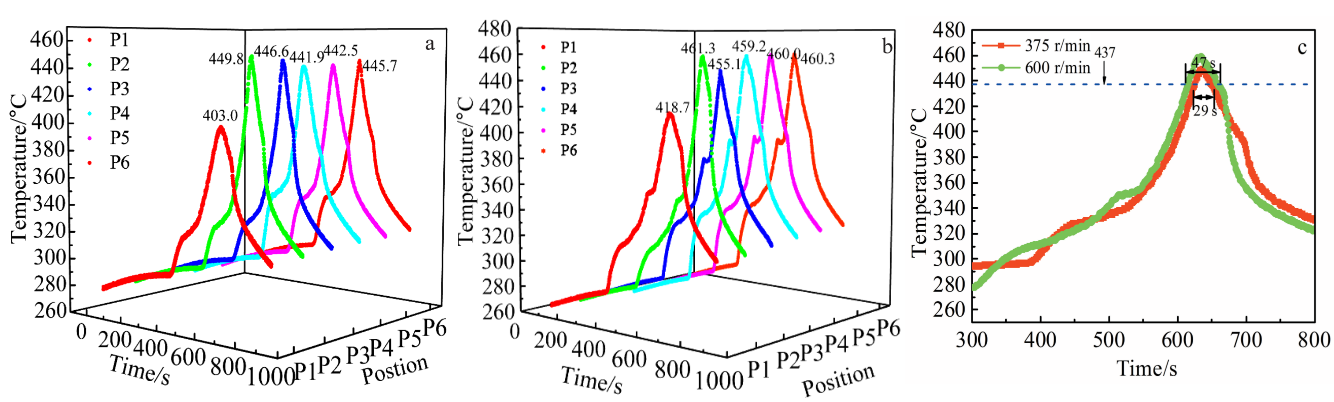

Fig.2 Thermal cycle curves at 375 r/min (a) and 600 r/min (b); peak temperature and residence time for P2 (c)

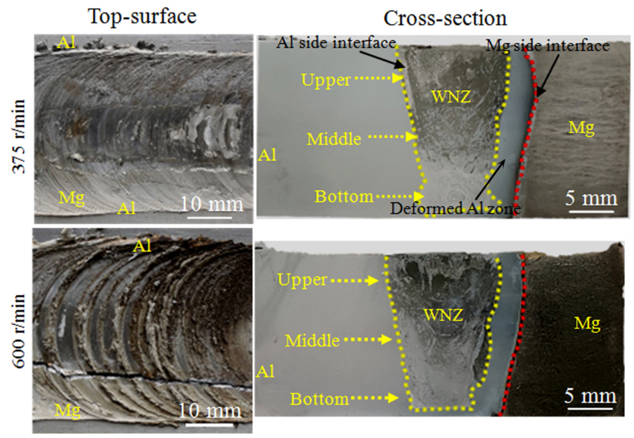

Fig.3 Top-surface and cross-section morphologies of Al/Mg joints at 375 r/min and 600 r/min

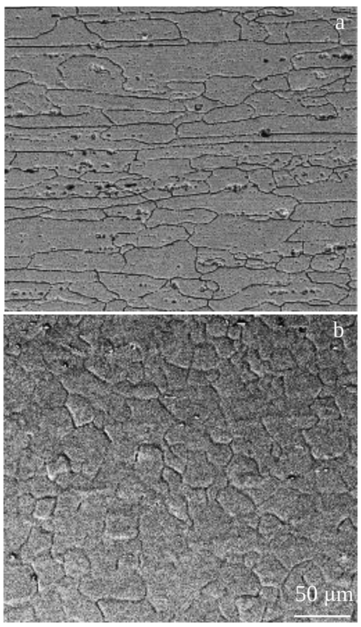

Fig.4 Microstructures of as-received base material: (a) 5A06-H112 Al alloyand (b) AZ31B-O Mg alloy

the Al_3Mg_2 layer suggests that intensive dislocation forms in the interior of the Al_3Mg_2 layer. These dislocations provide a path for Al atoms and Mg atoms to diffuse into the Al_3Mg_2 layer. Wang et al[28] also confirmed that dislocations at the interface may contribute to the diffusion of Fe atoms into IMC by TEM and EDS. Moreover, whether at the middle or at the bottom of the Al side, the higher KAM value is obtained for the fine Al grains rather than the boundary of the TMAZ and the WNZ, as can be seen in Fig.6e and 6f.

The SEM images and corresponding band contrast maps of the Mg side interface along the thickness direction are shown in Fig.8. It can be seen from Fig.8a that a eutectic layer with 38.83 μm in thickness exists at the Mg side interface. Through further EDS and EBSD analysis, the layer is composed of Mg solid solution and $Al_{12}Mg_{17}$ phase. The raindrop-like Mg solid solution is embedded in the $Al_{12}Mg_{17}$ phase. This result indicates that the eutectic reaction ($Mg+Al_{12}Mg_{17} \leftrightarrow$ Liquid) occurs at the upper of the Mg side interface. Moreover, a continuous and columnar Al_3Mg_2 IMC layer, with 12.3 μm in thickness and oriented normal to the boundary between the Al_3Mg_2 layer and eutectic layer, appears on the right side of this eutectic layer, as can be seen from Fig. 8a. From these characteristics of microstructure and composition near the Mg side interface, it can be reasonably inferred that the Al_3Mg_2 phase firstly nucleates at the interface with DRXed Al grains and then continues to grow along the preferred direction, which is perpendicular to the interface. This phenomenon is also confirmed in diffusion bonding between Al and Mg conducted by Wang et al[29].

Fig.8b presents the microstructure of the middle on the Mg side interface. The middle interface is composed of two layers of IMCs, namely the Al_3Mg_2 layer and $Al_{12}Mg_{17}$ layer, rather than the eutectic layer composed of Mg solid solution and $Al_{12}Mg_{17}$. The chemical composition of the bottom interface is the same as that of the middle. Nevertheless, the average total thickness of the IMCs at the middle is 18.92 μm which is slightly larger than the total thickness of 13.30 μm at the bottom.

Fig.9 shows the KAM maps of the Mg side interface along the thickness direction. As shown in Fig.9a, the largest degree of KAM is located at the Al_3Mg_2 layer near the Mg side interface, indicating that the Al_3Mg_2 layer has the largest plastic strain. For the middle and bottom of the Mg side interface, the KAM value of the IMC layer is also larger than

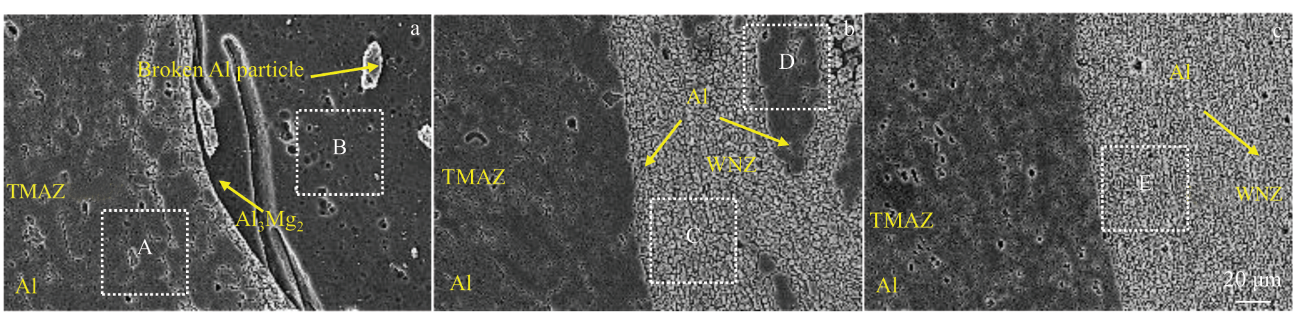

Fig.5 SEM images of the Al side interface along the thickness direction at 375 r/min: (a) upper, (b) middle, and (c) bottom

Table 2 EDS analysis of chemical composition for the positions marked in Fig.5 (at%)

Position	Al	Mg	Possible phase
A	92.43	7.57	Al
B	60.83	39.17	Al_3Mg_2
C	89.69	10.31	Al
D	89.84	10.16	Al
E	88.12	11.88	Al

that of the Al and Mg matrix. The mismatched interface between the Al_3Mg_2 layer with high plastic strain and the Al layer with low strain is prone to produce tensile stress due to rapid heating and rapid cooling during the FSW process, eventually resulting in cracks along this interface, as can be seen in Fig.8.

2.3.2 High rotational speed

Fig. 10 presents the SEM images of the Al side interface along the thickness direction at 600 r/min. The EDS results are

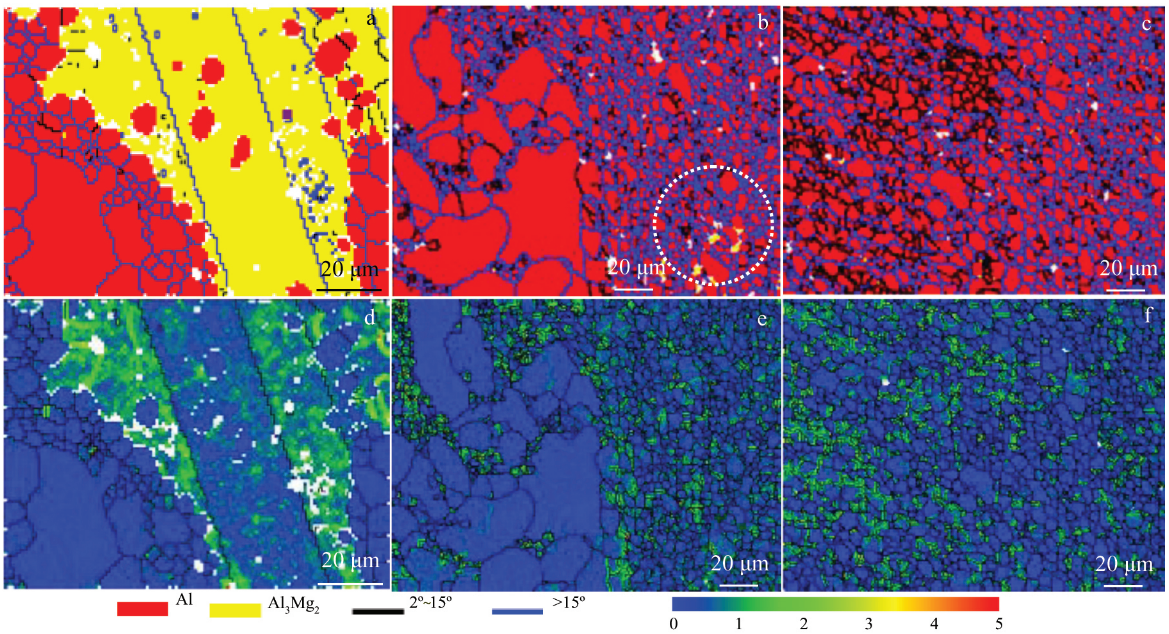

Fig.6 EBSD phase distribution maps (a~c) and KAM maps (d~f) of the TMAZ/WNZ interface along the thickness direction: (a, d) upper, (b, e) middle, and (c, f) bottom

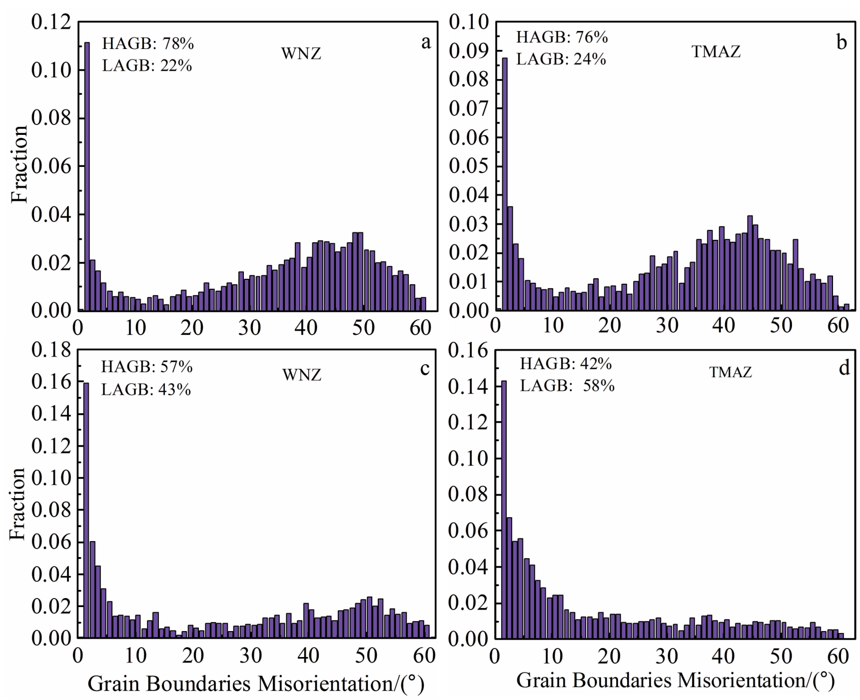

Fig.7 Grain boundary misorientation of WNZ (a, c) and TMAZ (b, d) near the Al side interface: (a, b) middle and (c, d) bottom

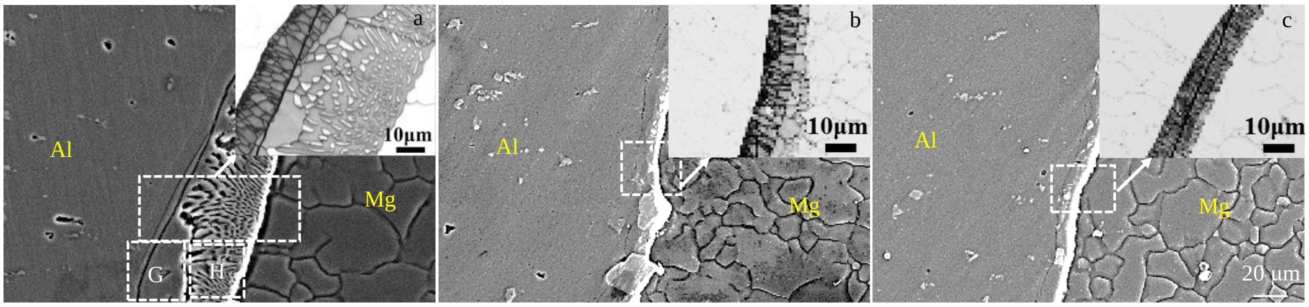

Fig.8 SEM images and band contrast maps of the Mg side interface along the thickness direction at the 375 r/min: (a) upper, (b) middle, and (c) bottom

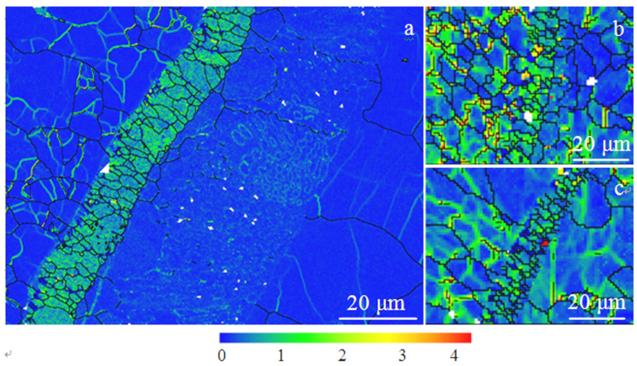

Fig.9 KAM maps of the Mg side interface along the thickness direction: (a) upper, (b) middle, and (c) bottom

also given in Table 3 for analysis of the phase constitution in this joint. Same as the upper on the Al side interface at 375 r/min, the upper interface at 600 r/min is also composed of broken Al particles and coarse Al_3Mg_2 phases, as shown in Fig.10a and Table 3. It can be seen from Fig.10b that a large amount of fine Al particles and large-size Al_3Mg_2 phases near the interface are distributed at the middle on the Al side interface. Note that at a low rotational speed of 375 r/min, as mentioned in Fig.5b, the microstructures of the WNZ near the middle and bottom interface on the Al side have merely fine Al particles, but many coarse Al_3Mg_2 phases appear at 600 r/min. This result is mainly related to temperature, strain rate and material mixing caused by different rotational speeds. Chen et al[30] found that the thickness of IMCs increases with the increase of the strain rate and temperature. Venkateswaran and Reynolds[31] reported that the high rotational speed can determine the formation of well-developed material mixing when the Al/Mg FSW is conducted.

The SEM images of the Mg side interface along the thickness direction at 600 r/min are presented in Fig. 11. Combined with the EDS results in Table 3, the Mg interface is composed of the eutectic layer ($Mg+Al_{12}Mg_{17}$) and the Al_3Mg_2 layer along thickness direction. As can be seen from Fig.11, the Al/Mg joint obtained at 600 r/min fractures along the boundary between the TMAZ (consisting of fine Al grains) and the Al_3Mg_2 layer. The average thickness of the Al_3Mg_2 layer and eutectic layer on the upper of the Mg side interface is 32.89 and 68.92 μm, respectively. At the middle, the average thickness of the Al_3Mg_2 layer and the eutectic layer decreases to 14.55 and 62.44 μm, respectively. The Al_3Mg_2 layer with an average thickness of 12.56 μm and the eutectic layer with an average thickness of 57.07 μm are obtained in the bottom. It can be concluded that the thickness of the Al_3Mg_2 layer and eutectic layer decreases from the upper to the bottom. Compared with the microstructure on the Mg side at 375 r/min, it can be found that the thickness of the eutectic layer increases significantly in the same thickness direction at 600 r/min. In addition, the thickness of the Al_3Mg_2 layer at 600 r/min increases significantly compared with that at 375 r/min.

3 Discussion

3.1 Effect of rotational speed on the low melting point eutectic and IMCs

Firouzdor and Kou[20] mentioned that the heat input during

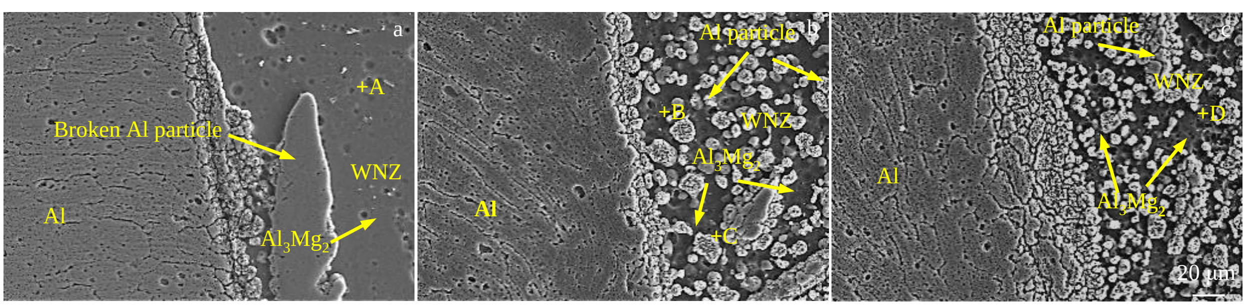

Fig.10 SEM images of the Al side interface along the thickness direction at 600 r/min: (a) upper, (b) middle, and (c) bottom

Table 3 EDS analysis of chemical composition for the positions marked in Fig.10 and Fig.11 (at%)

Position	Al	Mg	Possible phase
A	59.99	40.01	Al_3Mg_2
B	67.62	32.38	$Al+Al_3Mg_2$
C	85.53	14.47	Al
D	62.91	37.09	Al_3Mg_2
E	59.19	40.81	Al_3Mg_2
F	37.58	62.42	$Mg+ Al_{12}Mg_{17}$
G	60.92	39.08	Al_3Mg_2
H	61.87	38.13	Al_3Mg_2

FSW is close to the welding parameters and torque. The total heat input generated by tool rotation and travel in FSW is expressed as follows:

$$Q = Q_\omega + Q_F = \frac{2\pi\omega}{60}\int_0^t M\mathrm{d}t + \frac{v}{60}\int_0^t F_x\,\mathrm{d}t \tag{1}$$

where Q is the total heat input (J), Q_ω is the heat input (J) provided by tool rotation, Q_F is the heat input (J) provided by tool travel, ω is the rotational speed (r/min), t is time (s), M is the welding torque (N·m), v is the welding speed (mm/min), and F_x is the force (N) acted by tool in the welding direction (x). Firouzdor and Kou[20] proposed that the heat input from tool rotation Q_ω is much higher than Q_F from tool travel. Therefore, the total heat input can be simplified as[32]:

$$Q = Q_\omega = \frac{2\pi\omega}{60}\int_0^t M\mathrm{d}t = \frac{2\pi\omega lM}{v} \tag{2}$$

where l is the welding length (mm).

In this experiment, welding speed is a constant value of 23.5 mm/min. The heat input increases with the increase of the rotational speed according to Eq.(2). As shown in Fig.2a and 2b, the peak temperature increases as the rotational speed varies from 375 r/min to 600 r/min. Meanwhile, the high temperature residence time of the thermal cycle is significantly extended when a higher rotational speed is used. When the peak temperature of the interface exceeds 437 °C, the eutectic reaction will occur at the interface. The interdiffusion rate between Al and Mg atoms in liquid state is higher than in solid state, which causes the thicker eutectic layer to grow faster in liquid state[33].

Wang and Prangnell[29] reported that the high peak temperature and long residence time can promote the growth of IMCs. When the IMC layer is excessively thick, the bond between it and the matrix becomes poor, namely brittle and hard[34]. Therefore, the Al/Mg interface at 600 r/min is very weak and the fracture occurs after welding.

3.2 Effect of strain rate on the growth of IMCs

As described in Fig. 8 and Fig. 11, dissimilar Al/Mg FSW produces thick IMC layer along the interface, and its thickness gradually decreases from the upper to the bottom of this interface. The following is an in-depth analysis of the growth of the IMC layer. Based on the previous analysis, the formation of the IMC layer is controlled by the diffusion reaction. The relationship between the thickness of the IMC layer (d) and diffusion time (t) is described by the one-dimensional kinetic equation[35]

$$d = \sqrt{Dt} \tag{3}$$

$$D = D_0 \exp\left(\frac{-Q}{RT}\right) \tag{4}$$

$$t = \frac{-\Phi_{\text{shoulder}}}{v} \tag{5}$$

where D is the rate constant, D_0 is the pre-exponential factor, Q is the activation energy, R is the gas constant, T is the absolute temperature, Φ_{shoulder} is the diameter of the shoulder, and v is the welding speed.

Wang et al[29] reported that D_0 and Q of the Al_3Mg_2 phase formed during interdiffusion in Al/Mg weld joint are 8.01×10^{-8} m^2/s and 72 kJ/mol, respectively; D_0 and Q of the $Al_{12}Mg_{17}$ phase are 0.32 m^2/s and 168 kJ/mol, respectively. The diffusion time (t) is about 102 s by substituting shoulder diameter (Φ_{shoulder}=40 mm) and welding speed (v=23.5 mm/min) used in this experiment. Here, the absolute temperature T is taken as the average temperature in the middle of the Mg side interface at 375 r/min during the diffusion time of 102 s, which is about 693 K. According to the above calculated results, substituting them into Eq. (3), the thicknesses of Al_3Mg_2 layer and $Al_{12}Mg_{17}$ layer are approximately 5.52 and 2.66 μm. However, the measured thicknesses of Al_3Mg_2 layer and $Al_{12}Mg_{17}$ layer are 12.01 and 6.83 μm, respectively. Similarly, Panteli et al[36] used the parabolic kinetic growth law to predict the thickness of the IMC layer and the calculated thickness was about 50% of the measured thickness. The main reason for this difference is that the effect of the plastic

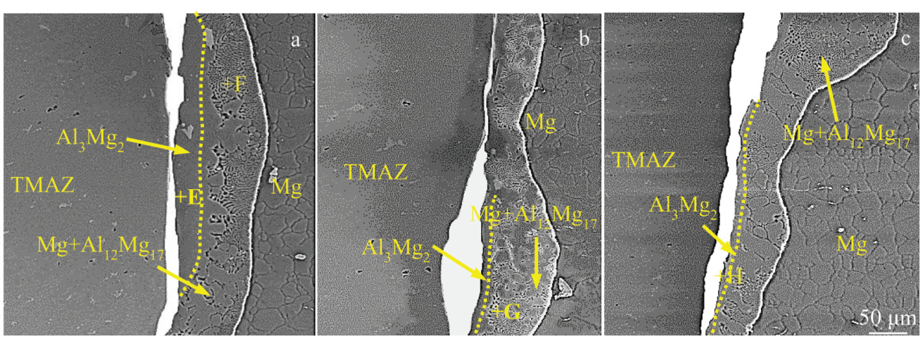

Fig.11 SEM images of the Mg side interface along the thickness direction at 600 r/min: (a) upper, (b) middle, and (c) bottom

deformation is not considered, and parabolic kinetic growth law is only applicable for the state of low strain rate.

Since the severe plastic deformation occurs on the Mg side interface of the Al/Mg FSW, the final microstructures such as IMCs and fine grains not only depend on the welding temperature, but also on the strain rate. The strain rate $\dot{\varepsilon}$ during the FSW can be evaluated by Eq.(6)[37].

$$\dot{\varepsilon} = \frac{R_m 2\pi r_e}{L_e} \tag{6}$$

where r_e and L_e are the average radius and length of dynamically recrystallized zone, respectively; R_m is the half of the rotational speed. In this experiment, the r_e at the upper, the middle and the bottom is 7.5, 6.3, and 5.4 mm, respectively. The L_e at the upper, the middle and bottom is 4, 10, and 18 mm, respectively. By substituting these values into Eq.(6), the strain rates at the upper, the middle and the bottom are calculated as 36.82, 12.37 and 5.89 s^{-1}, respectively.

Mahto et al[38] reported that the high strain rate can enhance the interdiffusion rate of Al and Fe atoms during the Al/Fe FSW. In addition, Tang[39] and Wang et al[28] also mentioned that severe plastic deformation causes significant reduction of the vacancy migration energy and vacancy formation energy[40], resulting in higher diffusion coefficient. Simultaneously, the dislocations during the FSW provide a channel for the diffusion of dissimilar atoms because of high strain rate deformation. Therefore, the thickness of IMC layer at the upper side interface at high strain rate is larger than that of the middle interface at low strain rate.

4 Conclusions

1) As the rotational speed increases from 375 r/min to 600 r/min, both the peak temperature and residence time increase. The increase of the heat input of the weld joint will cause thicker layer of IMCs and low melting point eutectic.

2) The Al_3Mg_2 layer either on the Al side interface or on Mg side interface has high KAM value, which indicates larger dislocation density in the Al_3Mg_2 layer.

3) The strain rate has a significant influence on the growth of the IMCs. High strain rate can enhance the diffusion and eventually cause thicker IMCs. Besides, the thickness of the IMCs at different thicknesses along the Mg side interface is also related to the strain rate.

References

1 Deng H, Chen Y, Zhang T *et al*. *Materials Letters*[J], 2019, 255: 126543

2 Hu W, Ma Z, Ji S *et al*. *Journal of Marterials Science and Technology*[J], 2020, 53: 41

3 Choi J W, Liu H, Ushioda K *et al*. *Materials Characterization* [J], 2019, 155: 109 801

4 Ma Z Y, Feng A H, Chen D L *et al. CRC Critical Reviews in Solid State Sciences*[J], 2018, 43(4): 269

5 Fu B, Qin G, Li F *et al*. *Journal of Materials Processing Science Technology*[J], 2015, 218: 38

6 Lv X, Wu C S, Yang C *et al. Journal of Materials Processing Technology*[J], 2018, 254: 145

7 Li P, You G, Wen H *et al. Journal of Materials Processing Technology*[J], 2019, 264: 55

8 Kwon Y J, Shigematsu I, Saito N. *Materials Letters*[J], 2008, 62: 3827

9 Ji S, Meng X, Liu Z *et al. Materials Letters*[J], 2017, 201: 173

10 Suhuddin U F H, Fischer V, dos Santos J F. *Scripta Materialia* [J], 2013, 68: 87

11 Yamamoto N, Liao J, Watanabe S *et al*. *Materials Transactions* [J], 2009, 50: 2833

12 Azizieh M, Sadeghi A, Abbasi M *et al*. *Materials Chemistry and Physics*[J], 2016, 170: 251

13 Sato Y S, Park S H C, Michiuchi M *et al*. *Scripta Materialia*[J], 2004, 50: 1233

14 Mclean A A, Powell G L F, Brown I H *et al*. *Science and Technology of Welding and Joining*[J], 2013, 8: 462

15 Ouyang J, Yarrapareddy E, Kovacevic R. *Journal of Materials Processing Technology*[J], 2006, 172: 110

16 Firouzdor V, Kou S. *Metallurgical and Materials Transactions A* [J], 2010, 41: 3238

17 Yu M R, Zhao H Y, Jiang Z H *et al. Journal of Materials Science & Technology*[J], 2019, 35: 1543

18 Su H L, Harmelin M, Donnadieu P *et al*. *Cheminform*[J], 1997, 28: 57

19 Gerlich A, Su P, North T H. *Science and Technology of Welding and Joining*[J], 2005, 10: 647

20 Firouzdor V, Kou S. *Metallurgical and Materials Transactions A* [J], 2010, 41: 2914

21 Zhao Y, Jiang S, Yang S *et al*. *The International Journal of Advanced Manufacturing Technology*[J], 2016, 83: 673

22 Buffa G, Baffari D, Di Caro A *et al. Science and Technology of Welding and Joining*[J], 2015, 20: 271

23 Chen S, Li X, Jiang X *et al. Materials Science and Engineering A*[J], 2018, 735: 382

24 Etter A L, Baudin T, Fredj N *et al*. *Materials Science and Engineering A*[J], 2007, 445: 94

25 Imam M, Sun Y F, Fujii H *et al. Metallurgical and Materials Transactions A*[J], 2017, 48: 208

26 Moradi M M, Jamshidi Aval H, Jamaati R *et al. Journal of Manufacturing Processes*[J], 2018, 32: 1

27 Mahto R P, Pal S K. *Journal of Manufacturing Processes*[J], 2020, 55: 103

28 Wang T, Sidhar H, Mishra R S *et al. Materials & Design*[J], 2019, 174: 107 795

29 Wang Y, Prangnell P B. *Materials Characterization*[J], 2017, 134: 84

30 Chen B, Wang Y, Xiao C *et al. Materials Science and Technology* [J], 2017, 34: 703

31 Venkateswaran P, Reynolds A P. *Materials Science and Engineering A*[J], 2012, 545: 26

32 Yu M, Zhao H, Jiang Z *et al*. *Journal of Materials Science & Technology*[J], 2019, 35: 1543
33 Liang Z, Qin G, Ma H *et al. Science and Technology of Welding and Joining*[J], 2016, 22: 363
34 Baghdadi A H, Sajuri Z, Selamat N F M *et al. International Journal of Minerals Metallurgy and Materials*[J], 2019, 26: 1285
35 Xu L, Robson J D, Wang L *et al. Metallurgical and Materials Transactions A*[J], 2018, 49: 515
36 Panteli A, Robson J D, Brough I *et al. Materials Science and Engineering A*[J], 2012, 556: 31
37 Chang C I, Lee C J, Huang J C. *Scripta Materialia*[J], 2004, 51: 509
38 Mahto R P, Kumar R, Pal S K. *Materials Characterization*[J], 2020, 160: 110 115
39 Tang J, Chen L, Zhao G *et al. Journal of Alloys and Compounds*[J], 2019, 784: 727
40 Wang C Y, Jiang Y B, Xie J X *et al. Materials Science and Engineering A*[J], 2017, 708: 50

转速对铝/镁搅拌摩擦焊接头金属间化合物及低熔点共晶的影响

徐 洋[1]，柯黎明[1,2]，毛育青[2]，陈 宜[2]
(1. 西北工业大学 凝固技术国家重点实验室，陕西 西安 710072)
(2. 南昌航空大学 轻合金加工科学与技术国防重点学科实验室，江西 南昌 330063)

摘 要：研究了转速对铝/镁搅拌摩擦焊接头金属间化合物和低熔点共晶的影响，并用电子背散射衍射表征了铝侧和镁侧界面微观结构。结果表明，当采用375 r/min的低转速时，镁侧界面上部出现由Mg固溶体和$Al_{12}Mg_{17}$相组成的共晶层，平均厚度为38.83 μm。在镁侧界面上部还发现一层厚度为12.3 μm的连续柱状Al_3Mg_2层，垂直于Al_3Mg_2层与共晶层的边界。在镁侧界面的中部和底部，只有Al_3Mg_2层和$Al_{12}Mg_{17}$层，其厚度沿厚度方向从上到下依次减小。此外，铝侧和镁侧界面的Al_3Mg_2层具有较高的平均晶粒取向差，这为铝和镁原子间的扩散提供了一条途径。当转速为600 r/min时，Mg固溶体与$Al_{12}Mg_{17}$相组成的共晶层沿厚度方向分布在镁侧界面上，共晶层厚度较低转速（375 r/min）时显著增加。镁侧界面上部的Al_3Mg_2层和共晶层的平均厚度分别为32.89和68.92 μm。最后，由转速引起的应变速率对金属间化合物的生长起着重要作用。

关键词：金属间化合物；低熔点共晶；厚板铝/镁接头；搅拌摩擦焊；旋转速度

作者简介：徐 洋，男，1991年生，博士生，西北工业大学凝固技术国家重点实验室，陕西 西安 710072，E-mail：xuyang_010101@126.com